Journal of Inorganic and General Chemistry
ZAAC
Zeitschrift für anorganische und allgemeine Chemie
www.zaac.wiley-vch.de
RESEARCH ARTICLE
DOI: 10.1002/zaac.202200048

PbTe/PbSe Thermoelectric Nanocomposites: The Impact of Length Modulations on Lowering Thermal Conductivity

Daniele Selli,[a, d] Davide Donadio,[b] and Stefano Leoni*[c]

Dedicated to Prof. Mercouri Kanatzidis on the Occasion of his 65th Birthday

PbTe and PbSe are among the most promising thermoelectric materials used in the mid-temperature (400–900 K) power generation range. In these materials the efficiency increase in thermoelectric performance is critically related to the lowering of lattice thermal conductivity (κ_L), without compromising the electronic power factor. By means of state-of-the-art equilibrium molecular dynamics (EMD), we investigate heat transport in several nanostructured PbTe/PbSe models as a function of material morphology. Layered composites show a reduction of the average κ_L of about 35% with respect to the bulk. The insertion of PbSe nanoparticles into a PbTe matrix, or viceversa PbTe into PbSe reduces κ_L by up to 45% while in more anisotropic nanocomposites the reduction exceeds PbSe/PbTe alloys. Layered composites show the lowest lattice thermal conductivity in the direction of layer stacking, for which an optimal thickness is identified. Along this line we provide a full account of the impact of alloying and (sub)nanostructuring on heat transport for this important class of materials. Particularly anisotropic nano-dot morphologies and layered (sub)nanocomposites emerge as a paradigm for outstanding thermoelectric materials.

Introduction

The increased energetic demand and climate changes due to fossil fuel combustion call for an integral effort towards a sustainable development. Heat harvesting from battery packs, fuel cell modules or photovoltaic cells have become central for increased efficiency in energy conversion. Finding high-performance thermoelectric materials capable of directly and reversibly convert heat to electrical energy is therefore a task of top priority.[1–6] The efficient control of thermoelectric energy conversion processes relies on the ability to assemble materials with tailored thermal transport properties.[7] The thermoelectric efficiency at a given temperature (T) is expressed by a dimensionless figure of merit $ZT = S^2\sigma T/\kappa$. Here S is the Seebeck coefficient, σ is the electrical conductivity, and κ is the thermal conductivity, which in turn is the sum of lattice and electronic contributions $\kappa = \kappa_L + \kappa_{el}$. This expression suggests a large Seebeck coefficient and high electrical conductivity as requirements for good thermoelectric materials, besides a low thermal conductivity. Nonetheless, these conditions cannot be immediately translated into a design strategy, mainly due to the interdependence of the physical parameters giving the ZT expression.

In binary lead chalcogenides thermal conductivity is dominated by the lattice contribution (κ_L), while the electronic part remains comparatively small. In this class of compounds phonon scattering is typically achieved by impurity modes or alloying, which effectively lower thermal conductivity.[7,8] PbTe is a good thermoelectric material in the so-called intermediate temperature regime (500–900 K, ZT (600 K) = 0.9).[1,9] Single-crystalline PbTe nanowires grown by chemical vapor transport show reduced thermal conductivity.[10] The thermal conductance of 180 nm diameter, micrometer long PbTe nanowire is around 11 nW/K at 300 K, ~10^3 times smaller than that of an equally thick layer of bulk PbTe.[11] Different from bulk compounds, nanocomposites, endotaxial precipitates, mesoscale grain boundary engineering and heterogeneous multiphase materials are emerging paradigms for a broader scattering of phonon heat transport.[12–15] Along this line Hsu *et al.* achieved exceptionally high ZT ~ 2.2 at 800 K in LAST ($AgPb_mSbTe_{2+m}$) alloys.[12] Enhanced ZT is observed in PbTe/$PbSe_xTe_{1-x}$ quantum dot superlattice structures, with a value of ZT ~ 2 at ambient temperature.[13] Nanostructured PbTe-PbS materials are prepared by spinodal decomposition and nucleation-and-growth techniques, with thermal conductivity values as low as κ_L ~ 0.4 W/m K.[16] Together with nanostructuring, the

[a] *D. Selli*
Technische Universtät Dresden, Institut für Physikalische Chemie, D-01062 Dresden, Germany
[b] *D. Donadio*
Department of Chemistry, University of California, Davis, Davis, California 95616, USA
[c] *S. Leoni*
Cardiff University, School of Chemistry, Park Place, CF10 3AT, Cardiff, UK
E-mail: leonis@cf.ac.uk
[d] *D. Selli*
VTA Austria GmbH, Umweltpark 1, A-4681 Rottenbach, Austria

Supporting information for this article is available on the WWW under https://doi.org/10.1002/zaac.202200048

presence of Tl impurity levels in p-doped PbTe leads to a doubling of ZT (ZT ~ 1.5) at 773 K.[17]

In PbTe based materials the good thermoelectric performance is largely due to the low lattice thermal conductivity. However, Te is not only rare in the Earth's crust but also increasingly used in a number of other applications, such as steel metallurgy, solar cells, phase change materials for digital recording, and thermoelectric cooling devices based on Bi_2Te_3.[18] Attractive Te-free alternatives to rock-salt PbTe are the congeneric PbSe and PbS, which have remarkably similar electronic and structural properties.[19,20] Furthermore, even if PbSe-based materials usually have a lower figure of merit in the mid temperature range (around 500 K) compared to PbTe, in doped PbSe the Seebeck coefficient does not exhibit the usual[19] "turn-over" at high temperature, but keeps increasing even at 1000 K, thus making it a good alternative to PbTe especially at higher temperatures, owing also to its higher melting point.[20]

Despite existing paradigms, a controlled design of thermoelectric materials remains an involved task. Atomistic simulations may represent the method of choice towards a deeper understanding of the thermoelectric phenomenon, as they provide the necessary resolution for elucidating the impact of defects, the role of interfaces, nanostructuring and morphology.[21] Furthermore, calculations can provide benchmark values to assist the difficult experimental task of measuring thermal transport, in particular in nanoscale materials.[23,24] In this work, we investigate the atomistic details of (sub) nanostructuring on lowering thermal conductivity in PbTe–PbSe mixed systems, using solid solutions (alloys) as reference systems. We use equilibrium molecular dynamics (EMD) simulations to compute the thermal conductivity of several PbSe/PbTe systems. The systems considered are PbTe–PbSe solid solutions of different composition ($PbTe_{0.25}Se_{0.75}$, $PbTe_{0.50}Se_{0.50}$, $PbTe_{0.75}Se_{0.25}$), PbTe/PbSe layered superlattices (Figure 1a) and PbSe (PbTe) spherical precipitates of variable diameter embedded in a PbTe (PbSe) matrix (Figure 1b). The latter comprises spherical inclusions of different size (Figure 1c) and dense nano-dot geometries ("eight-in-a-box") (Figure 1d).

Methods

The realistic modeling of materials strongly benefits from the use of empirical interaction potentials of simple analytical form, which allow the simulation of much larger systems over longer time scales, compared to methods based on first principles. For binary semiconducting materials a simple interatomic potential was shown to very reliably account for structural and elastic properties, and to be very accurate even in the description of phase transitions.[25] Nevertheless, the restricted number of available parameters limits this approach. Additionally, parameters adapted to binary compounds must be transferable to mixed system, which is rarely the case. To provide suitable potentials for heat transport calculations in PbSe/PbTe, transferable potentials for the binary compounds PbSe and PbTe were parameterized. The interaction between the atoms was described by a sum of Lennard-Jones (LJ) and Coulomb terms:

$$U_{ij}(r_{ij}) = U_{Coul}(r_{ij}) + U_{LJ} = \frac{q_i q_j}{4\pi\varepsilon_0 r_{ij}} + 4\varepsilon_{ij}\left[\left(\frac{\sigma_{ij}}{r_{ij}}\right)^{12} - \left(\frac{\sigma_{ij}}{r_{ij}}\right)^{6}\right]$$

Here r_{ij} is the distance between atoms i and j; ε_{ij} and σ_{ij} are the LJ parameters; q_i and q_j are partial charges on atoms i and j; and ε_0 is the dielectric constant of vacuum. Only LJ coefficients of pairwise equal atoms are fitted, as cross terms were obtained from Lorentz – Berthelot mixing rules. For PbSe, an existing set of parameters was taken from literature.[26] Therein, four LJ coefficients and partial charges (5 parameters in total) were fitted to lattice parameter and elastic constants. In this work ε_{ij} LJ coefficients were refitted using the GULP[27] code, to additionally reproduce the thermal conductivity κ_L of PbSe at room temperature (300 K) and its temperature dependence (300–1200 K).[28] To construct transferable parameter sets, ε_{ij} and σ_{ij} of Te were fitted on PbTe lattice and elastic constants using Pb parameters from PbSe, again ensuring that the parameter reliably accounted for PbTe thermal conductivity as known from experiment.[29] Calculated elastic and lattice constants for both PbTe and PbSe bulk are in good agreement with previous results.[30,31] The values of κ_L at 300 K are 1.98 ± 0.07 W/mK (PbSe) and 1.69 ± 0.08 W/mK (PbTe), in good agreement with DFT/BTE calculations[32] and experiments.[33,34] Moreover the predicted temperature dependence of κ_L compares very well with available reference experimental data (Figure 2).[30,31] The κ_L of solid solutions is also closely reproduced (Figure S1). Details of the potential parameters and fitting procedures can be found in the Supporting Information.

The lattice thermal conductivity κ_L, was calculated using the Green-Kubo (GK) relation based on the fluctuation-dissipation theorem:[35]

$$\kappa_l = \frac{1}{k_b V T^2}\int_0^{\infty} \frac{\langle \boldsymbol{J}(t)\cdot\boldsymbol{J}(0)\rangle}{3} dt$$

where k_b is the Boltzmann constant, V is the volume of the system, T is the temperature and $\langle \boldsymbol{J}(t)\cdot\boldsymbol{J}(0)\rangle/3$ is the heat current autocorrelation function averaged over three directions. The heat current vector for a pair potential is defined as:[36]

$$\boldsymbol{J} = \sum_i^N \varepsilon_i v_i + \frac{1}{2}\sum_{i,j;i\neq j}^N (\sigma_{ij}\cdot v_j)$$

where ε_i and v_i are the site energy and velocity associated with atom i, respectively. The 3x3 tensor σ_i denotes the atomic virial stress.

Results

Different kinds of convergence tests have been performed. The truncation time (t_{tr}) chosen to evaluate the integral in the Green-Kubo relation in Eq. 2 was tested on a reference system,

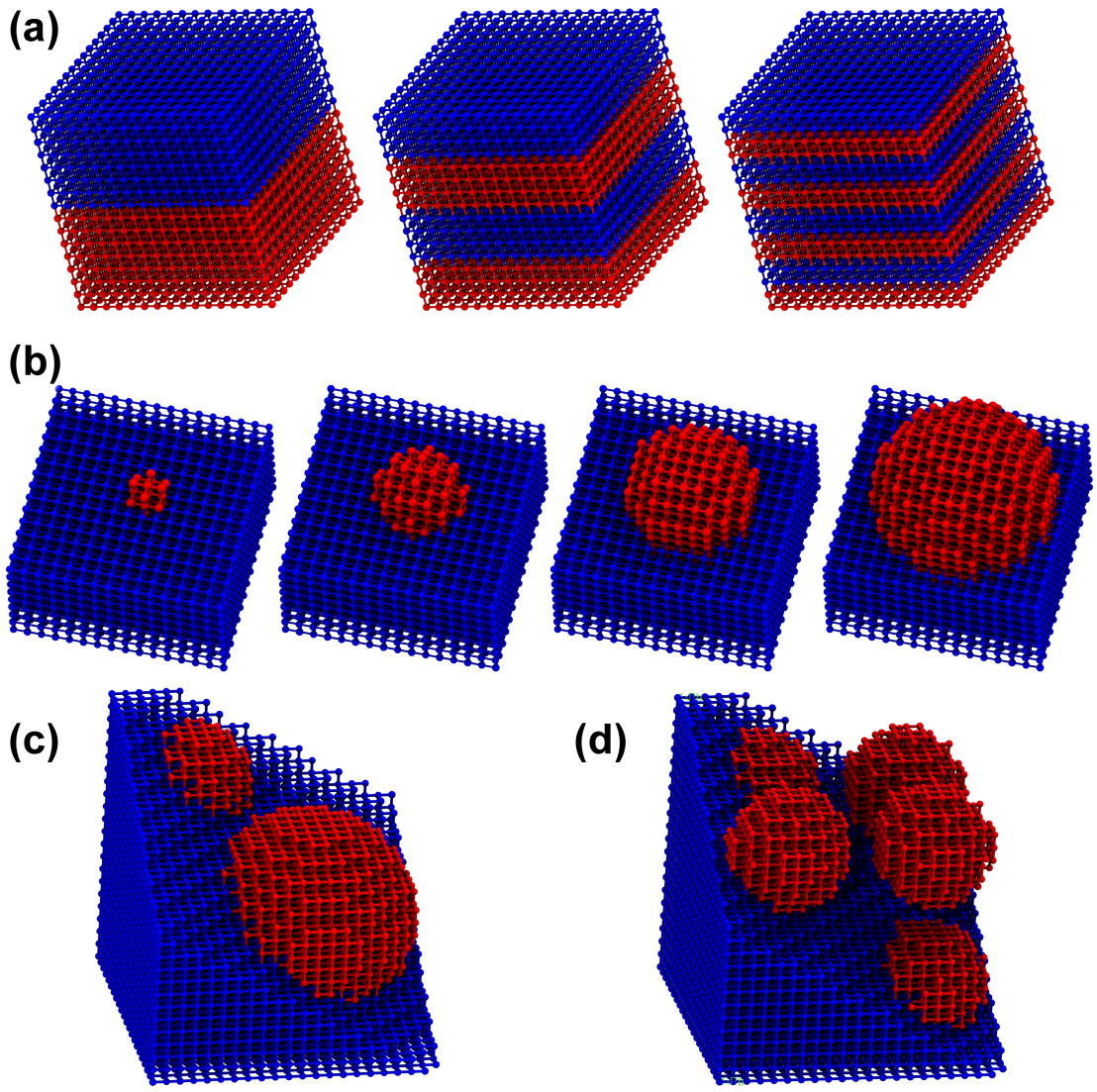

Figure 1. (a) Layered structure of PbTe (in blue) and PbSe (in red) in their rock-salt modification. Layers are (from, left to right) 25, 12.5 and 6.25 Å thick. (b) Intercalated PbTe(Se) spheres in a PbSe(Te) matrix. Sphere radii are, from left to right 5, 10, 15 and 20 Å, respectively. (c) 25 Å and 15 Å radius spheres and (d) "eigth-in-a-box" spheres of 15 Å radius.

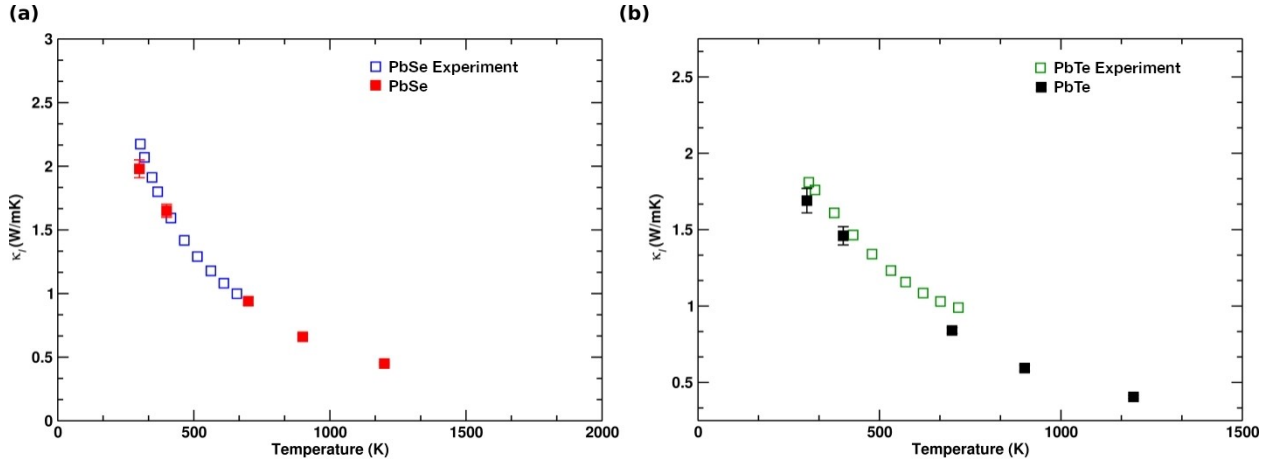

Figure 2. Predicted lattice thermal conductivity of bulk PbSe (a) and PbTe (b) in comparison with experimental counterpart values.[30,31]

the solid-solution composition $PbSe_{0.50}Te_{0.50}$ with 4096 atoms in the cell, considered in this work (see Figure S2 in the Supporting Information). After t_{tr} = 40 ps the values calculated for κ_L converged. Size-dependence effects were investigated as well. This is necessary as the small size of the simulation box may affect the computed value of the thermal conductivity. For semiconductors this is of relevance as low frequency phonons may have long mean free paths, which provide a significant contribution to κ_L.[7] Supercells containing up to ~10^5 atoms, i.e. 4x4x4 replicas of the original nanostructured systems (~10^3 atoms), were considered. The values calculated from supercells are equal within standard deviations (Figure S3), while linear regression lines are parallel in the size range considered, meaning that relative values of thermal conductivity for the different geometries may be already acceptable for small cells (4096), while in larger cells (~10^4) size effects become negligible. Top performing nanocomposites were therefore evaluated in a large simulation box containing 10648 atoms, as this size represents a viable compromise between size effect impact and computational efficiency (results are shown in Table 1). Nonetheless, systematic calculations in a small cell of 4096 atoms were used to identify trends towards best candidates, as it is summarized in Table S3. Accordingly, at room temperature alloys display lower thermal lattice conductivity than binary phases. The $PbSe_{0.50}Te_{0.50}$ solid solution in particular shows maximal reduction, in agreement with previous works based on first principles methods.[37] The best performing layered systems features 1.25 nm thick layers, while in the compounds with nanoinclusion the largest nano-dots more effectively reduce lattice thermal conductivity, with PbTe precipitates in PbSe matrix being preferable.

Although at room temperature alloys are competitive or even better than both systems with nano-inclusions and superlattices, the value of κ_L of bulk PbSe and PbTe and of nanostructured materials rapidly approaches the one of the best alloy as temperature is increased (Figure S4a–c). The lattice thermal conductivity of layered superlattices is strongly anisotropic at room temperature, as κ_z is markedly lower than κ_x ($\kappa_y \cong \kappa_x$). This anisotropy rapidly disappears as a function of temperature. Already at 400 K the κ_z/κ_x ratio reaches 0.51 and at higher temperature it is close to 1, since increased anharmonic three-phonon scattering takes over phonon scattering at the interfaces. Nonetheless κ_z remains below the values of the $PbTe_{0.50}Se_{0.50}$ alloy by as much as ~25% (Figure S4c). In contrast with nanoinclusion compounds κ_z is not a monotonic function of the superlattice spacing. The observed trends of κ_L as a function of size and dimensionality in PbTe and PbSe systems show analogies with Si/Ge superlattices.[38] In both cases, for ~1 nm lattice spacing 2D geometries provide a more efficient reduction of κ_L, but even lower thermal conductivity can be achieved using larger nano-dots. Similarly to Si/Ge systems the crossover of κ_L between 2D and 0D nanostructures occurs beyond 3 nm.[38]

The κ_L of samples with smaller nano-dots (radius from 0.5 to 1 nm) is of the order of that of bulk PbTe and PbSe, whereas a significant reduction of κ_L is obtained from larger nano-inclusions (1.5 or 2 nm, Table S3). The effect of enlarging the sphere diameter is more prominent in the case of PbTe spheres into a PbSe matrix than vice versa. A trend of lattice thermal

Table 1. Average lattice thermal conductivity (300 K) computed for PbTe(PbSe) spheres into PbSe(PbTe) matrices, alloy (50/50 Te/Se) and 12.5 Å thick layered structure for systems containing 10468 atoms in the simulation box. Values are in units of W/mK. For sphere inclusions, the sphere-sphere distance is indicated. The distance **d** between two spheres is defined in Figure 3b.

Sphere (Te in Se)	300 K	Distance d (Å)
10 Å radius	2.07 ± 0.06	55
15 Å radius	1.88 ± 0.09	45
20 Å radius	1.65 ± 0.05	38
25 Å radius	1.25 ± 0.06	24
30 Å radius	1.16 ± 0.03	13
"eight-in-a-box"15 Å radius	1.04 ± 0.05	9
"different size", 15 Å and 25 Å	1.45 ± 0.09	
Sphere (Se in Te)		
10 Å radius	2.94 ± 0.22	55
15 Å radius	2.47 ± 0.12	45
20 Å radius	2.21 ± 0.13	38
25 Å radius	1.75 ± 0.09	24
30 Å radius	1.33 ± 0.08	13
"eight-in-a-box", 15 Å radius	1.13 ± 0.08	9
"different size", 15 Å and 25 Å	1.59 ± 0.06	
Alloy		
50%/50% Te/Se	1.06 ± 0.03	
Layered, 12.5 Å		
x	1.44 + 0.07	
y	1.47 + 0.13	
z	0.74 + 0.03	
Total	1.22 + 0.06	

conductivity reduction as a function of size of embedded spheres is thus emerging (Figure S5). However, since cells of 4096 atoms limit the maximal host sphere radius to 2 nm, the investigation was extended to the larger cell of 10648 atoms. The trend of κ_L for sphere radii between 1 nm and 3 nm for different system sizes (4096 vs 10648) are compared in Figure S5. Enlarging sphere sizes has a reduced impact on lowering lattice thermal conductivity. The spacing between spheres is rather the relevant parameter here. Table 1 summarizes values of κ_L at ambient temperature (300 K) for large cell systems (10648): single sphere inclusions, two spheres with different size (Figure 1c) and "eight-in-a-box" PbSe(Te) nanocomposites in PbTe(Se) matrices (Figure 1d) are compared to the best-performing $PbSe_{0.50}Te_{0.50}$ alloy with the same size. Narrowing the distance between nano-dots (as shown in Figure 3b) causes lattice thermal conductivity to decrease. With reference to Figure 3a, the trend of κ_L reduction as a function of size eventually yields a value of κ_L smaller than the best 50% solid solution, underpinning the relevance of the (sub)nano-regime for devices.

The "eight-in-a-box" spheres PbTe nanocomposites in a PbSe matrix represents the right balance between dot size and inter-dot distance. The resulting enhanced phonon scattering lowers lattice thermal conductivity to values smaller than the best alloy. Temperature dependence for these two systems has been investigated and is reported in SI, Figure S6. The decrease of κ_L in the alloy is close to monotonic, while nanostructured compounds display a rather step-like trend. In particular, at ambient and higher temperatures the inclusion of nano-dots is predicted to lower thermal conductivity to a larger extent than the best alloy compound.

Discussion

In order to understand the physics behind changes in thermal conductivity between our samples and bulk binary compounds, effective mean free paths of carriers as a function of frequency were computed. The size of larger systems of 10648 atoms per simulation box rapidly becomes too demanding with respect to memory allocation of the dynamical matrix. Therefore only 4096 atom systems were considered. We compared values for PbSe bulk (the case of PbTe shows qualitatively the same results with a shift at lower frequencies due to larger Te atomic mass, see SI, Figure S7) with the one obtained for the $PbSe_{0.50}Te_{0.50}$ alloy, the largest PbTe sphere (20 Å of diameter) embedded in a PbSe matrix and the 12.5 Å thick layered structure.

The effective mean free path of mode *i* is given by $\lambda_i = \nu_i^g \tau_i$ where effective group velocities ν_i^g were obtained by diagonalizing the dynamical matrix of the system, and lifetimes τ_i were computed by MD simulations from the normalized autocorrelation function of the energy (E) of each vibrational mode *i*: $\tau_i = \int_0^\infty \langle E_i(t) \cdot E_i(t0)\rangle / \langle E_i(0) \cdot E_i(t0)\rangle dt$ (details of each calculation can be found in the Supporting Information, Figs. S8-S9).[38,39] Figure 4 shows the impact of (sub)nanostructuring on thermal conductivity. From frequencies of $\nu \approx 1$ THz on, a significant average decreasing of the mean free path with respect to bulk PbSe is clearly visible. In the interval 1 THz $\leq \nu \leq$ 3 THz, value reductions by a factor ~350 are found for the alloyed structure, ~310 for PbTe nanoparticles embedded in a PbSe matrix, while the layered structure outstands the previous ones by a factor as large as $\lambda_z \sim 550$ along the stacking direction ($\lambda_x = \lambda_y \sim 40$), in agreement with the trend of lattice thermal conductivity reduction shown in Table 1. The same analysis allows discriminating among layered nanocomposites. Comparing the mean free path for the 6.25 Å thick layered structure to the one with a thickness of 12.5 Å (Figure S10), the latter is distinguished by a markedly lower thermal conductivity across

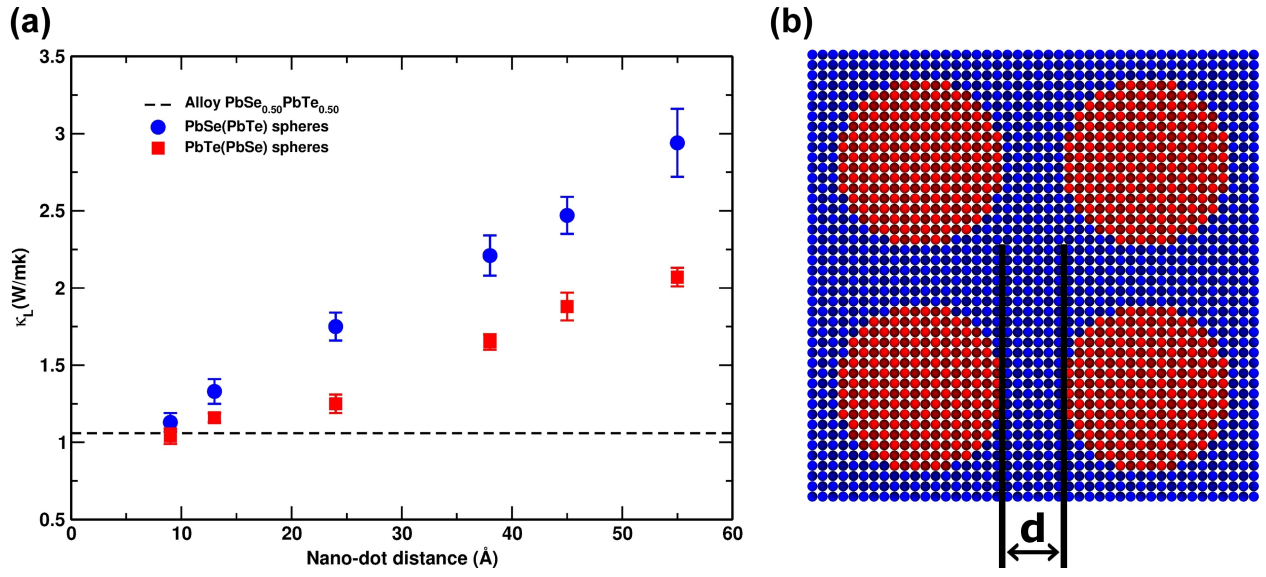

Figure 3. (a) Lattice thermal conductivity dependence of PbTe(PbSe) and PbSe(PbTe) as a function of nano-dot distance **d** (b).

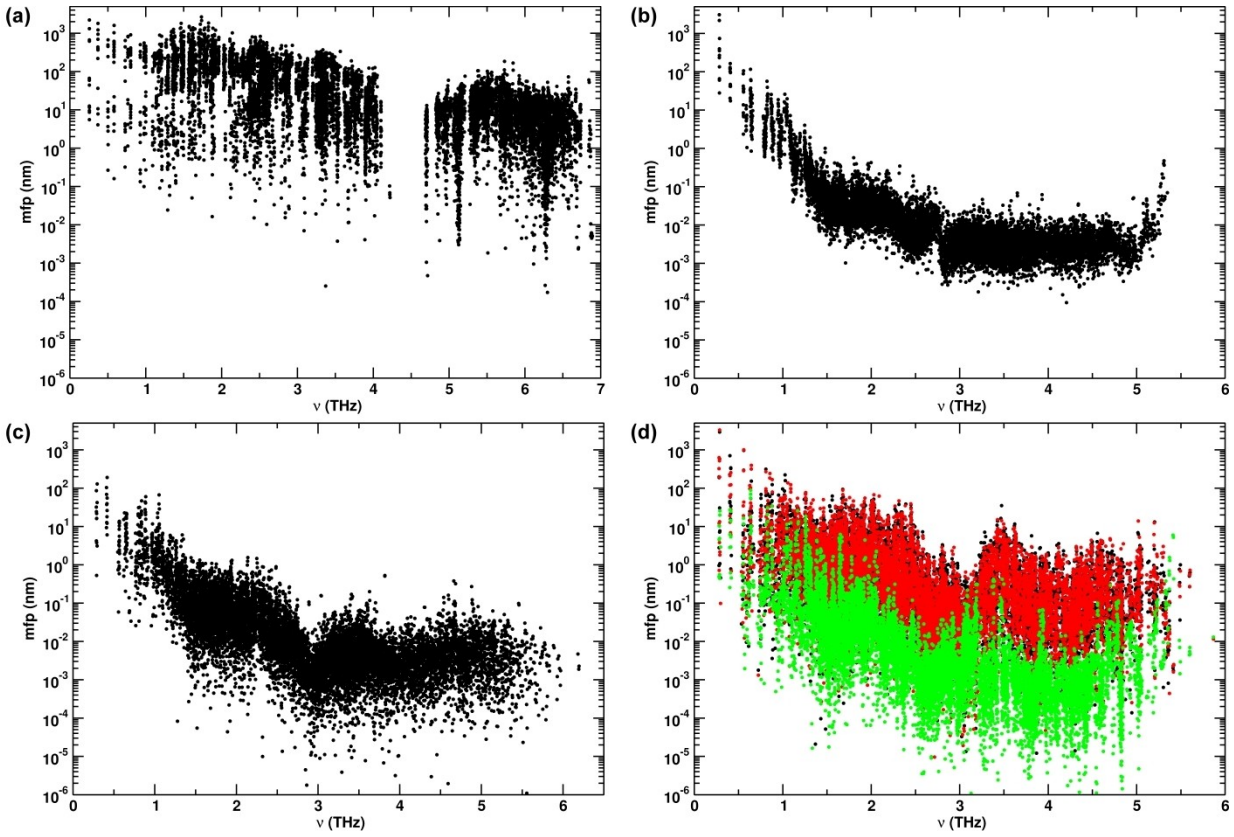

Figure 4. Average mean free path of vibrational modes as a function of frequency for bulk PbSe sample (a), $PbTe_{0.50}Se_{0.50}$ alloy (b), 20 Å radius PbTe sphere in PbSe matrix (c) and directional mean free path for 12.5 Å thickness layer structure (4096 atoms in the simulation box) (d); colors (black, red, green) correspond to x, y and z directions.

the layers. This in turn is due to a reduction of the mean free path of intermediate frequency modes, which suggests that a selective filtering on selected portions of the frequency range can be achieved as a function of morphological features of the composite. While the right scale of (sub)nanocompositing may be difficult to guess by trial and error, the computational approach of the present work is very precise in indicating a viable route for a systematic improvement of thermoelectric materials. While on the one hand our approach confirms the enhancement of the thermoelectric figure of merit for PbTe-PbSe solid solutions,[1,40–41] it opens on the other hand a more promising and "intelligent" nanoengineering approach for the creation of specific geometries and interfaces. At room temperature, the insertion of PbTe(Se) nanoparticles into PbSe(Te) matrix causes a reduction of κ_L up to 45% with respect to the binary compound, while in layered nanocomposites the rather modest average reduction of about 35% for in-layer conduction is remarkably enhanced above 60% perpendicular to the layers. Furthermore, the study of lager systems suggests densely packed nano-dot as nanoengineering design targets. This qualifies nanocomposites with stong anisotropic features and dense packing as potentially outstanding thermoelectrics for renewable energy applications.

Our results indicate the overall decreasing of the thermal lattice conductivity in nanocomposites with respect to PbTe or PbSe to arise from a reduction of the mean free path of modes at selected frequency. PbTe-PbSe alloys are known to enhance thermoelectric efficiency because of phonon features, which are distinct from the binary phases. Our computational approach sheds light on a different strategy of thermal conductivity reduction, that is engineering at the (sub)nanometer scale. Along this line it is possible to obtain structures with potentially better phonon scattering properties. Experimentally[42] κ_L resulted independent from layer thickness between 5 and 50 nm. Our calculations indicate that the threshold for an effect to set in has to be at shorter length values, also pinpointed by the indication of densely packed nano-dots spaced by less than a few nanometers. Considering group velocities, lifetimes and mean free path of low frequency vibrational modes of different layered structures, an optimal spacing between different species (alternating PbTe and PbSe layers) can be identified, which enhances anisotropy and reduces thermal conductivity along the layer stacking direction. Low values are also found if spherical PbTe nanoparticles are growth inside a PbSe matrix (or vice versa), as an alternative means to modulate material distribution and length sequences on the (sub)nano scale. Experimentally, ordered assemblies of nanocrystals can be obtained on a length scale compatible with these predictions.[43]

Conclusions

This large-scale atomistic study of the priority material class of lead chalcogenides has provided a systematic investigation of size effects in PbSe/PbTe composites. By means of equilibrium MD calculations, lowest lattice thermal conductivity values were shown to be characteristic of a region between solid solutions ("0" nm) and nanostructured (~5 nm) materials. Length modulations in this region (i.e. between 0 and 5 nm) achieve efficient scattering of intermediate frequency modes. The precise reproduction of experimental curves and the precise evaluation of the temperature dependence of thermal conductivity as a function of morphological features provide guidance for the design of novel materials with improved properties. We expect our approach to be widely applicable for thermal transport evaluation, and for designing better thermoelectric materials.

Supporting Information

Details on transferable pair potential parameters for PbSe and PbTe, heat autocorrelation function, size validation, mean free paths for bulk, PbSe and PbTe, lifetimes and mean free paths for PbTe composites are provided as supplementary material.

Author Contributions

The manuscript was written through contributions of all authors. All authors have given approval to the final version of the manuscript.

Acknowledgements

S.L. and D.S. thank the DFG for financial support within SPP 1415. We thank the Center for Information Services and High-Performance Computing (ZIH) at TU Dresden for the generous allocations of computer time. S.L. gratefully acknowledges support from the DFG in form of a Heisenberg Scholarship (Heisenberg Program). S.L. thanks ARCCA Cardiff for computational resources.

Conflict of Interest

The authors declare no conflict of interest.

Data Availability Statement

The data that support the findings of this study are available from the corresponding author upon reasonable request.

Keywords: Thermal transport · lead tellurides · lead selenides · nanomaterials · molecular dynamics · thermoelectrics

[1] J. G. Snyder, E. S. Toberer, *Nat. Mater.* **2008**, *7*, 105.
[2] G. Chen, M. S. Dresselhaus, G. Dresselhaus, J. P. Fleurial, T. Caillat, *Int. Mater. Rev.* **2003**, *48*, 45.
[3] J. Sootsman, D. Y. Chung, M. G. Kanatzidis, *Angew. Chem. Int. Ed.* **2009**, *48*, 8616.
[4] D. M. Rowe, CRC Handbook of Thermoelectrics: Macro to Nano, CRC/Taylor & Francis, **2006**.
[5] M. Zebarjadi, K. Esfarjani, M. S. Dresselhaus, Z. Ren, G. Chen, *Energy Environ. Sci.* **2012**, *5*, 5147.
[6] C. Han, Q. Sun, Z. Li, S. X. Dou, *Adv. Energy Mater.* **2016**, *6*, 1600498–1.
[7] K. Biswas, J. He, I. D. Blum, C.-I Wu, T. P. Hogan, D. N. Seidman, V. P. Dravid, M. G. Kanatzidis, *Nature* **2012**, 489, 414.
[8] M. G. Kanatzidis, *Chem. Mater.* **2010**, *22*, 648.
[9] C. Wood, *Rep. Prog. Phys.* **1988**, *51*, 459.
[10] J. W. Roh, S. Y. Jang, J. Kang, S. Lee, J.-S. Noh, W. Kim, J. Park, W. Lee, *Appl. Phys. Lett.* **2010**, *96*, 103101.
[11] M. Fardy, A. I. Hochbaum, J. Goldberger, M. M. Zhang, P. Yang, *Adv. Mater.* **2007**, *19*, 3047.
[12] C. Hsu, F. Loo, F. Guo, W. Chen, J. Dyck, C. Uher, T. Hogan, E. Polychroniadis, M. G. Kanatzidis, *Science* **2003**, *303*, 818.
[13] T. C. Harman, P. J. Taylor, M. P. Walsh, B. E. LaForge, *Science* **2002**, *297*, 2229.
[14] K. Biswas, J. He, Q. Zhang, G. Wuang, C. Uher, V. P. Dravid, M. G. Kanatzidis, *Nature Chem* **2011**, *3*, 160.
[15] S. A. Yamini, D. R. G. Mitchell, Z. M. Gibbs, R. Santos, V. Patterson, S. Li, Y. Z. Pei, S. X. Dou, G. J. Snyder, *Adv. Energy Mater.* **2015**, *21*, 1501047.
[16] J. Androulakis, C. Lin, H. Kong, C. Uher, C. Wu, T. Hogan, B. A. Cook, T. Caillat, K. M. Paraskevopoulos, M. G. Kanatzidis, *J. Am. Chem. Soc.* **2007**, *129*, 9780.
[17] J. P. Heremans, V. Jovovic, E. S. Toberer, A. Saramat, K. Kurosaki, A. Charoenphakdee, S. Yamanaka, G. J. Snyder, *Science* **2008**, *321*, 554.
[18] R. Venkatasubramanian, E. Siivola, V. Colpitts, B. O'Quinn, *Nature* **2001**, *413*, 597.
[19] I. I. Ravich, B. A. Efimova, I. A. Smirnov, *Semiconducting lead chalcogenides*; Plenum Press: New York, 1970.
[20] D. Parker, D. Singh, *J. Phys. Rev. B* **2010**, *82*, 035204.
[21] T. G. Alekseeva, E. A. Gurieva, P. P. Konstantinov, L. V. Prokof'eva, M. I. Federov, *Semiconductors* **1996**, *30*, 1125.
[22] B. Jiang, Y. Yu, H. Chen, J. Cui, X. Liu, L. Xie, J. He, *Nat. Commun.* **2021**, *12*, 3234.
[23] D. Selli, S. E. Boulfelfel, P. Schapotschnikow, D. Donadio, S. Leoni, *Nanoscale* **2016**, *8*, 3729.
[24] D. G. Cahill, W. K. Ford, K. E. Goodson, G. D. Mahan, A. Majumdar, H. J. Maris, R. Merlin, S. R. Phillpot, *J. Appl. Phys.* **2003**, *93*, 793.
[25] W. Grünwald, A. Zayak, J. B. Neaton, P. L. Geissler, E. Rabani, *J. Chem. Phys.* **2012**, *136*, 234111(1-6).
[26] P. Schapotschnikow, M. A. van Huis, H. W. Zandbergen, D. Vanmaekelbergh, T. J. H. Vlugt, *Nano Lett.* **2010**, *10*, 3966.
[27] J. D. Gale, *Phil. Mag. B* **1996**, *73*, 3.
[28] J. Androulakis, D.-Y. Chung, X. Su, L. Zhang, C. Uher, T. C. Hasapis, E. Hatzikraniotis, K. M. Paraskevopoulos, M. G. Kanatzidis, *Phys. Rev. B* **2011**, *84*, 155207.
[29] J. He, L.-D. Zhao, J.-C. Zheng, J. W. Doak, H. Wu, H.-Q. Wang, Y. Lee, C. Wolverton, M. G. Kanatzidis, V. P. Dravid, *J. Am. Chem. Soc.* **2013**, *135*, 4624.
[30] Y. Zhang, X.-Z. Ke, C.-F. Chen, J. Yang, P. R. C. Kent, *Phys. Rev. B* **2009**, *80*, 024304.
[31] B. Qiu, H. Bao, G. Q. Zhang, Y. Wu, X. L. Ruan, *Comput. Mater. Sci.* **2012**, *53*, 278.
[32] J. M. Skelton, S. C. Parker, A. Togo, I. Tanaka, A. Walsh, *Phys. Rev. B* **2014**, *89*, 205203.

[33] A. A. El-Sharkawy, A. M. Abou El-Azm, M. I. Kenawy, A. S. Hillal, H. M. Abu-Basha, *Int. J. Thermophys.* 1983, 4, 261.
[34] G. A. Akhmedova, D. S. Abdinov, *Inorg. Mater.* **2009**, *45*, 854.
[35] D. A. McQuarrie, *Stat. Mech.*; University Science Books: Sausalito, CA, **2000**; p 642.
[36] G. A. Greene, Y. I. Cho, J. P. Hartnett, A. Bar-Cohen, *Adv. Heat Transfer*; Elsevier: New York, **2006**; pp 212–213.
[37] Z.-T. Tian, J. Garg, K. Esfarjani, T. Shinga, J. Shiomi, G. Chen, *Phys. Rev. B* **2012**, *85*, 184303.
[38] Y. He, D. Donadio, J.-H. Lee, J. C. Grossman, G. Galli, *ACS Nano* **2011**, *5*, 1839.
[39] I. Savic, D. Donadio, F. Gygi, G. Galli, *Appl. Phys. Lett.* **2013**, *102*, 073113.
[40] P. F. P. Poudeu, J. D'Angelo, H. Kong, A. Downey, J. L. Short, R. Pcionek, T. P. Hogan, C. Uher, M. G. Kanatzidis, *J. Am. Chem. Soc.* **2006**, *128*, 14347.
[41] A. F. Ioffe, *Semiconductor Thermoelements and Thermoelectric Cooling*; Infosearch: London, 1957.
[42] Y. K. Koh, C. J. Vineis, S. D. Calawa, M. P. Walsh, D. G. Cahill, *Appl. Phys. Lett.* **2009**, *94*, 153101.
[43] M. Brumer, A. Kigel, L. Amirav, A. Sashchiuk, O. Solomesh, N. Tessler, E. Lifshitz, *Adv. Funct. Mater.* **2005**, *15*, 1111.

Manuscript received: February 3, 2022
Revised manuscript received: March 29, 2022
Accepted manuscript online: April 11, 2022

RESEARCH ARTICLE

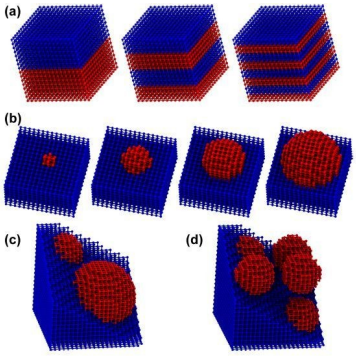

*D. Selli, D. Donadio, S. Leoni**